# The Role of the Fiber and Bond in Hygroexpansion and Curl of Paper

**August Brandberg (**KTH Royal Institute of Technology, CD Laboratory for Fiber Swelling and Paper Performance, Graz University of Technology)**, Hamid Reza Motamedian (**KTH Royal Institute of Technology, CD Laboratory for Fiber Swelling and Paper Performance, Graz University of Technology)**, Artem Kulachenko (**KTH Royal Institute of Technology, CD Laboratory for Fiber Swelling and Paper Performance, Graz University of Technology) and **Ulrich Hirn** (CD Laboratory for Fiber Swelling and Paper Performance, Graz University of Technology)

**ABSTRACT**
The underlying mechanism of hygroexpansion of paper products' deformation resides on the microscale and is a product of the coupling between hydrophilic fibers and micromechanical details of the fiber network, including the geometry and alignment of fibers and bonds. We present a micromechanical framework suitable for studying hygroexpansion from the fiber- and bond-level. Using the developed model, we show that due to the three-dimensionality of the bond, the transverse deformations of the fibers are not transferred effectively to the in-plane deformation of the sheet. At the same time, the longitudinal deformation of the fiber accounts for a large portion of the hygroexpansion even in highly oriented sheets. On the other hand, the out-plane deformation of paper is predominantly controlled by the strain gradient in the bonds which stems from transverse shrinkage or expansion of the fibers in the bond region. Therefore, considering the bonds as three-dimensional entities is vital for the analysis since a two-dimensional approximation overestimates the impact of the transverse deformation of the bonds to the in-plane properties and underestimates moisture-induced out-of-plane deformations of the fiber network.

**INTRODUCTION**

In-elastic strains due to environmental changes cause dimensional and performance variations, which can be strongly detrimental in many applications. While metals are mainly affected by in-elastic strains caused by temperature variations, cellulose products are most strongly affected by changes to the moisture content. These strains, collectively referred to as hygroscopic strains, are responsible for several types of dimensional instability such as curl and cockling [1]. Despite the persistent issues caused by hygroscopic strains, a unified theory explaining their cause and remedy has not been presented. However, thanks to previous work on the topic, many of the important pieces are understood.

Moisture-induced sheet instability stems from the competing mechanisms of mechanical compatibility of the fiber network and the strongly hydrophilic character of the single fiber, especially the amorphous cellulose regions. Since the network connectivity (and thus compatibility requirement) is formed primarily in the wet state prior to fibers shrinking, in-elastic strains, including hygroexpansion strains, are kept in balance by elastic strains causing stresses in the dry network.

The curl of paper sheets remains a problem in printing. Large ink volumes are attractive as they provide more vibrant colors, but when absorbing the ink fibers swell, causing the sheet to deform. This deformation often manifests in the form of curl. Modern sheet-fed printers have a curl control mechanism before allowing the sheet to pass through the printing unit. During two-sided printing, sheets which do not pass the curl control after printing on the first side have to be discarded together with several already printed sheets that follow it. In the worst case, a few troublesome sheets can produce a lot of waste.

One way to explain curl is to employ laminate theory. The wetted sheet has different through-thickness properties due to the varying degree of moisture content, and a layered formulation can be used to describe the strain gradient leading to bending. One of the first works employing this method was Carlsson [2], who obtained good results in the low to moderate curl regime. For larger deformations, the small-strain formulation employed by Carlsson is inadequate. Among the most prominent factors affecting the hygroexpansion are the fibers and their orientation, the density and drying restraints [3]. Laminate theory does not fully connect the observed behavior to the essential mechanisms driving the deformation of paper and is limited from the material development standpoint, even if these obstacles are not impossible to overcome as was shown later [4].

Another way to understand the changes brought on by changing the moisture content of the sheet is to directly consider the microscopic parts of the sheet. Such an approach to modeling the hygroscopic behavior of paper allows the constituents of paper (bonds, fibers, and network structure) to be modeled directly instead of via homogenization. In this way, it is possible to study the interactions of fibers and bonds in the presence of moisture and under a variety of minor and major changes to the sheet and the boundary conditions.

Micromechanical modeling begins with the microscopic observations by Page and Tydeman [5], as well as Nanko and co-authors [6, 7] and Uesaka and Qi [8]. These works showed clearly that fibers have an anisotropic swelling behavior, with most of the volumetric change taking place in the transverse direction by swelling of the fiber wall with comparatively minor longitudinal expansion. Uesaka and later Nanko observed the difference between the hygroexpansion of free and bonded fiber segments during constrained and free drying. Although the observations were restricted to surface fibers, it was clear that most of the deformation happens in the bonded areas of the fibers. Uesaka and Qi studied the impact of the individual bond configuration on the hygroexpansion and found that the stress-transfer ratio is strongly dependent on the configuration of the bond [8].

Uesaka [9] also developed general formulas for hygroexpansion based on the expression derived for multiphase elastic media by Dvorak and Benveniste [10]. Uesaka formulated a mean-field theory for the hygroexpansion of paper sheets based on the hygroexpansion of single fibers, expressed through the convenient notation of Equation (1)

$$\Sigma_{ij} = F_{ijkl}\sigma_{kl} \tag{1}$$

where $\Sigma_{ij}$ is the *ij*-th macroscopic stress component, $\sigma_{kl}$ is the *kl*-th microscopic stress component and $F_{ijkl}$ is the fourth-order tensor relating them. The formalism is essentially identical to that of Hooke's law, where stress and strain are likewise related by a fourth order tensor. Uesaka was able to explain several of the observed characteristics of paper curl, such as the effect of restraints, the effect of density and the difference in behavior between the MD and the CD. Later work by Salminen et al., employing a fiber network simulation tool confirmed that Uesaka's description of the micromechanics is to a large extent accurate [11].

Furthermore, Uesaka concluded that the hygroexpansivity of paper is governed both by the longitudinal and the transverse hygroexpansion of the fiber. This is contrary to the view that the hygroexpansion is mainly controlled by the transverse deformation of the fibers transferred through the bonds as the hygroexpansion in the CD is known to be significantly larger than in the MD. According to Uesaka, the hygroexpansion in the axial direction of the fiber accounts for up to 40% of the hygroexpansion in the CD direction even in highly oriented sheets [9]. This conclusion is not supported by two-dimensional (2D) network models in which the hygroexpansion of the fibers in the transverse direction is the dominant cause of macroscopic in-plane hygroexpansion [12].

Purely experimental research has been very valuable to characterize existing paper grades, their performance and to identify the main problems. However, due to the complexity of the problem and many parameters involved, factors related to the paper structure cannot be accurately controlled. In recent years, the fiber network was approached with micromechanical modeling and simulation methods. Bosco et al. developed a multiscale approach to study, among other things, irreversible shrinkage [13]. The bonded segment was modeled as a composite plate with in-plane stresses considered to be equal between the layers and the network considered to be 2D. Later work shows that neglecting the three-dimensional character of the bonds may lead to overestimation of their contribution in the response because of the through-thickness strain gradient in the bonded material [14]. In this work, we continue exploring the contribution of the bond to the in-plane and out-of-plane deformations.

Due to the inherent three-dimensionality, addressing curl with a micromechanical approach has not been attempted before as 3D micro-mechanical models tend to become computationally expensive. The relevant questions which may be addressed in a novel way are:

1. The creation and control of residual curl.
2. The effect of specimen size and geometry.

3. The effect of varying moisture profiles on curl.

We present a micromechanical framework suitable for modeling curl. It enables studying the underlying fiber- and bond-level mechanisms of hygroexpansion. The geometry of the network is reconstructed using fiber characterization tools and microtomography images of the network. The response of the network is computed using the non-linear finite element method, by which fibers are described using a series of beam elements, and the contact between fibers is modeled using a point-to-point contact. The hygroscopic strains are computed using a concurrent multiscale approach in which the fiber bonds are resolved at a smaller scale with a fully 3D model and then incorporated at the network level through inelastic strains. The proposed method allows the consideration of networks large enough to avoid boundary effects and includes inhomogeneities. The advances with respect to the previous works [11-13, 15] are as follows:

- The use of a 3D model to describe fiber network geometry and connectivity.
- The use of beam elements in conjunction with a concurrent multiscale approach to resolve the bond structure, which allows the study of hygroexpansion and provides a substantial reduction in computation time as compared to the use of solid or shell elements.

To verify the correctness of the implementation, we compare the results against a fully volumetric, 3D model. We then explore some of the results that can be produced when that implementation is employed on a large-scale network.

**METHOD**

Hygroexpansion strains appear because of the anisotropy of longitudinal and transverse deformation of fibers when subjected to moisture. The transverse hygroexpansion coefficients are known to be significantly greater than the longitudinal ones. The central question in any modeling scheme aiming to capture and explain in- and out-of-plane hygroexpansion is how to incorporate this anisotropy in the model while keeping the solution complexity at a level low enough to solve the problem in a reasonable time. The finite element method is used to analyze the network in this work. Fibers are discretized using 3-node geometrically nonlinear Timoshenko beam elements [16] with either solid or hollow rectangular cross-sections, and the inter-fiber bonds are simulated using beam-to-beam contact elements [17]. After a mesh convergence study, the element length is set to 40 μm. The section properties are computed at two quadrature stations along the beam by Gaussian integration over the cross-section (Figure 1). The constitutive equations including the hygro-induced strains are evaluated at every integration point. The coupling between torsional and axial deformation which can cause warping is neglected. The finite element equations are solved by an implicit time integration scheme in a quasi-static regime.

Prior to simulation and at the end of every converged sub-step, we probe the network and drop all fibers with only one or no connection to the rest of the network. Similarly, fiber bundles which are not connected to the boundary conditions imposed on the network are also dropped. In this way, the condition number of the stiffness matrix can be kept high throughout the simulation.

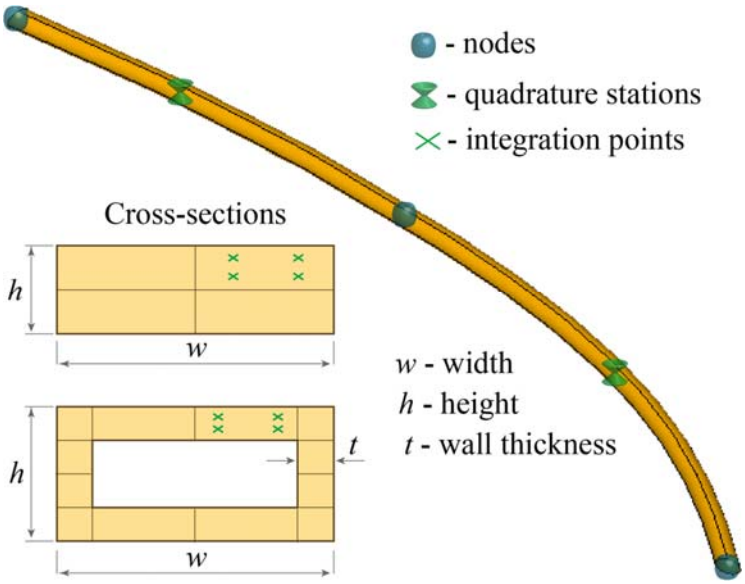


*Figure 1. Beam element topology and supported fiber cross-sections with depicted quadrature stations and integration points.*

Incorporating the effect of transverse deformation of one fiber on the longitudinal deformation of another is not possible in classical beam theory as the influence of normal strains oriented perpendicular to the longitudinal axis of the fiber is neglected. In order to overcome this limitation, we present a new technique which is based on a concurrent multiscale approach. To account for the load transfer between bonded fibers due to a shrinkage that is larger in the transverse direction than in the longitudinal, the bonds are simulated at a different scale using solid elements. We compute the strains arising due to hygro-deformations by resolving each bond with a detailed model based on the underlying geometry. The computed total strain in the bond is then transferred to the beam integration points with an interpolation procedure and introduced as inelastic strains. In this section, we describe the two analysis scales and the method used to transfer contributions from one scale to the other. This method allows a detailed study of:

1. The effect of paper structure (fiber orientation, anisotropy, density, two-sidedness).
2. The effect of water penetration dynamics, i.e. z-directional moisture gradients.
3. The effect of fiber morphology and mechanical properties of individual fibers.

**Modeling the effect of transverse hygroexpansion of one fiber on the longitudinal expansion of another**
We evaluate the contributions from each fiber-to-fiber bond in the network, using a bond-scale model created for that bond. The procedure is as follows:

1. The required data characterizing each bond are taken from the network database. This data includes geometrical dimension, material properties, moisture variation, etc.
2. Using the bond data, a model of the bond is created and analyzed using the finite element method. In this bond model, the fibers are assumed to be perfectly connected. Samples of such models are shown in Figure 2. As shown in the figure, the model can be 2D (Figure 2a), or 3D (Figure 2b).

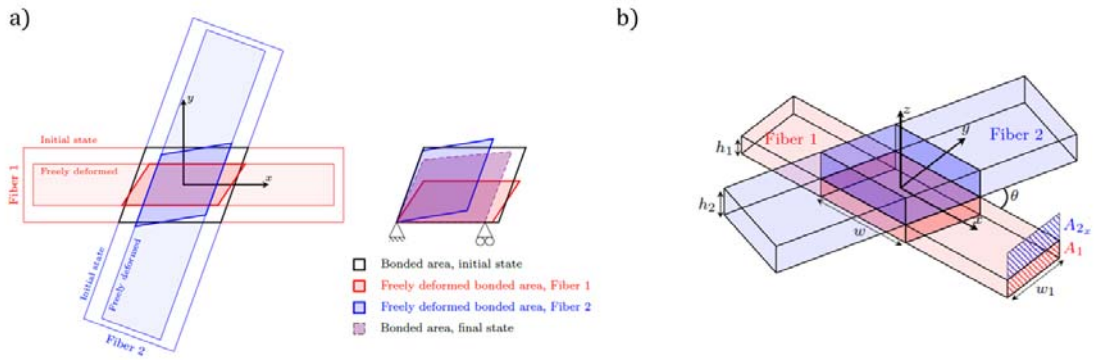


*Figure 2: Schematic description of the 2D (a) and 3D (b) bond model.*

3. The moisture variation distribution extracted from the network is applied to the bond model as an external load. The moisture variation results in a deformation state forming in the bond. As we use beam elements to model fibers at the network scale, we are interested in the longitudinal strain in each fiber, and we want to evaluate the part of the longitudinal strain induced by the transverse shrinkage/expansion of the other fiber. Assuming the applicability of superposition, we calculate the resulting strain as the difference between the total strain $\varepsilon_{tot}$ and the hygro-strain $\varepsilon_h$ that would appear if the segment was unconstrained by the other fiber. Assuming the relationship between moisture content and hygroscopic strain is linear as in Equation (2), the strain can be calculated as

$$\varepsilon_h = \varepsilon_{tot} - \beta_L \Delta mc \tag{2}$$

where $\beta_L$ is the longitudinal hygroexpansion coefficient and $\Delta mc = \Delta mc(x, y, z)$ is the change of moisture content at a point in space.

4. Next, this strain is transferred to the nodes of the beam element along which the bond is located. Contributions from multiple bonds along a beam element can be added, assuming that superposition is valid. To do so, we replace the local strain distribution at the bond (calculated using the bond-scale model) with a strain distribution along the whole beam element in such a way that the total strain energy stored in the element is not affected. For each beam element, we can express the total longitudinal strain energy by summing the contributions of all strains and integrating over the volume of the element as in Equation (3)

$$\begin{aligned} &\frac{1}{2}\int_0^{x_c-w/2}\left(\int_A \sigma_0\varepsilon_0 dA\right)dx + \frac{1}{2}\int_{x_c-w/2}^{x_c+w/2}\left(\int_A \sigma_0\left(\varepsilon_0+\varepsilon_h\right)dA\right)dx + \frac{1}{2}\int_{x_c+w/2}^{l}\left(\int_A \sigma_0\varepsilon_0 dA\right)dx \\ &= \frac{1}{2}\int_0^{l}\left(\int_A \sigma_0\left(\varepsilon_0+\overline{\varepsilon_h}\right)dA\right)dx \end{aligned} \tag{3}$$

where

- $\sigma_0$ and $\varepsilon_0$ are the current stress and strain in the element, caused by all factors except the transverse hygroexpansion of the other fiber at the bond,
- $\varepsilon_h$ is the strain at the bond site due to transverse hygroexpansion of the other fiber that we found by solving the bond-scale compatibility problem in step 3,

- $\overline{\varepsilon_h}$ is the resulting strain distribution across the whole beam element which consistently incorporates the hygroscopic strain $\varepsilon_h$ at the element level,
- $l$ is the element length,
- $w$ is the width of the bond, and
- $x_c$ is the location of the bond expressed in the element coordinate system such that $x_c / l$ describes the fraction of element length which is on one side of the bond and $\left(1 - x_c / l\right)$ describes the fraction of element length which is on the other side.

Such an equation is formulated and solved for $\overline{\varepsilon_h}$ in each of the elements containing a contact. Noting the symmetry in terms on the right and the left-hand side, we can simplify Equation (3) to:

$$\int_{x_c - w/2}^{x_c + w/2} \left( \int_A \sigma_0 \varepsilon_h dA \right) dx = \int_0^l \left( \int_A \sigma_0 \overline{\varepsilon_h} \right) dx \tag{4}$$

If we assume the actual strains can be approximated by a polynomial, we can express the strain throughout the beam in terms of the strains at specific points in the element weighted by the approximation functions chosen. As an example, if the fiber has a rectangular cross-section and we describe the spatial variation in the $x$, $y$ and $z$ directions using a linear distribution function, the strains at the corners of the volume can be used to describe the strains throughout the whole volume as

$$\left\{\varepsilon\right\} = \left\{\varepsilon\left(x, y, z\right)\right\} = \left[\mathbf{N}(x, y, z)\right]\left\{\varepsilon^{\mathrm{P}}\right\} \tag{5}$$

where

- $\left\{\varepsilon\right\} = \left\{\varepsilon\left(x, y, z\right)\right\}$ is a smooth spatial field describing the strains throughout the volume,
- $\left[\mathbf{N}\right]$ contains the approximation functions, and
- $\left\{\varepsilon^{\mathrm{P}}\right\}$ is a vector containing the particular solutions of the field at the points where we chose to solve the problem exactly.

This, in turn, allows us to express the longitudinal normal stress component as in Equation (6) where $E_L$ is the longitudinal Young's Modulus.

$$\sigma_0 = E_L \varepsilon_0 = E_L \left[\mathbf{N}\right]\left\{\varepsilon_0^{\mathrm{P}}\right\} \tag{6}$$

Assuming the same shape functions for $\overline{\varepsilon_h}$, we have:

$$\overline{\varepsilon_h} = E_L \left[\mathbf{N}\right]\left\{\overline{\varepsilon_h^{\mathrm{P}}}\right\} \tag{7}$$

Our goal is to find $\left\{\overline{\varepsilon_h^{\mathrm{P}}}\right\}$, a vector of strain values at some chosen points on the beam element. Finding this vector gives us a complete (albeit approximate) description of the strain distribution over the beam element. If we substitute Equation (6) and (7) into (4) we get the expression in Equation (8) which is clearly valid for any $\left\{\varepsilon_0^P\right\}$

$$\left\{\varepsilon_0^P\right\}^{\mathrm{T}} \int_{x_c-w/2}^{x_c+w/2} \left( \int_A E_L \left[\mathbf{N}\right]^{\mathrm{T}} \varepsilon_h dA \right) dx = \left\{\varepsilon_0^P\right\}^{\mathrm{T}} \int_0^l \left( \int_A E_L \left[\mathbf{N}\right]^{\mathrm{T}} \left[\mathbf{N}\right] dA \right) dx \left\{\overline{\varepsilon_h^{\mathrm{P}}}\right\} \tag{8}$$

and as a result, we end up with an expression relating the hygro-induced strain on the bond level with the hygro-induced strains on the fiber element level given by Equation (9). Note, $\left\{\overline{\varepsilon_h^{\mathrm{P}}}\right\}$ is a vector containing 8 values, one at each corner of the volume occupied by the beam.

$$\left\{\overline{\varepsilon_h^{\mathrm{P}}}\right\} = \frac{\int_{x_c-w/2}^{x_c+w/2} \left( \int_A E_L \left[\mathbf{N}\right]^{\mathrm{T}} \varepsilon_h dA \right) dx}{\int_0^l \left( \int_A E_L \left[\mathbf{N}\right]^{\mathrm{T}} \left[\mathbf{N}\right] dA \right) dx} \tag{9}$$

5. Finally, having the strain values at the nodes of the beam element, we interpolate them to the integration points across the beam and add them as inelastic strains to the constitutive relations. As $\left\{\overline{\varepsilon_h^{\mathrm{P}}}\right\}$ contains 8 values, the interpolated contribution to each integration point need not be the same in any of the spatial coordinates.

In the approach described above, we can use any polynomial as an approximation function. If a 2D bond model is used, then the spatial variation in the $z$-direction vanishes and the strain distribution at the bond, $\varepsilon_h$ is further simplified to

$$\varepsilon_h(x, y, z) = \varepsilon_h(x, y) \tag{10}$$

In the present work and examples that follow, we used bond models including some free segments of the fibers attached to the bond. We used both 2D and 3D bond scale FEM models and considered a linear strain distribution over the beam elements to transfer the effect of transverse deformations at the bonds to the network level calculations. The approach is integrated into a custom finite element code the details of which are presented in a series of publications [14, 17-19].

## RESULTS

The presentation of results is divided into three sections. First, we compare the proposed approach with a full 3D finite element model in which we employ volumetric elements. Since the 3D geometry of the network is difficult to reproduce exactly, we limit the comparison by considering only a single bond. In the second section, we benchmark the response of the 3D bond model against a 2D bond model when predicting in-plane hygrodimensional stability. In the third section, we explore the ability of the model to predict the out-of-plane deformation of paper.

### Comparison between a full 3D model and the proposed concurrent multiscale scheme

We will consider two crossing fibers. Each fiber will be represented as a beam with a solid rectangular cross-section in the beam model. The dimensions of the fibers are presented in Table 1. In the full 3D model, the fibers share the same geometry and are meshed with 8-node volumetric solid-shell elements [20]. The advantages of this element formulation are the ability to capture bending without shear or volumetric locking phenomena and to vary the number of integration points through the thickness which improves the accuracy of through-thickness solution fields such as moisture and strain gradients.

*Table 1. The geometrical and material properties of the fibers used in the comparison test.*

| | | |
|---|---|---|
| Fiber size, $\mu$m | Length | 300 |
| | Width | 30 |
| | Height | 9 |
| Modulus, GPa | Longitudinal | 20 |
| | Transverse | 3.5 |
| | Shear | 2.5 |
| Hygroexpansion coefficient, - | Longitudinal | 0.015 |
| | Transverse | 0.45 |

We assigned orthotropic material properties to the fibers in local coordinate systems (denoted with primes) aligned with the direction of the fiber and orientation of the cross-section (Figure 3). The material properties are listed in Table 1.

We consider fibers crossing at a straight angle. One end of each fiber is constrained while the other is free to move. In the beam model, the constraint is enforced on the nodal displacement as well as the rotation of the constrained nodes, whereas in the volumetric model only displacements are constrained. The net effect of this is nonetheless the same for both models. Figure 3 shows the total deformation due to a uniform moisture change of 15% for both the beam and solid-shell models. It is interesting to observe that out-of-plane deformations appear as a result of a uniform moisture change. The beam model shows reasonably close deformation at a computational cost reduced by an order of magnitude owing to the reduced number of degrees of freedom and therefore the size of the global stiffness matrix.

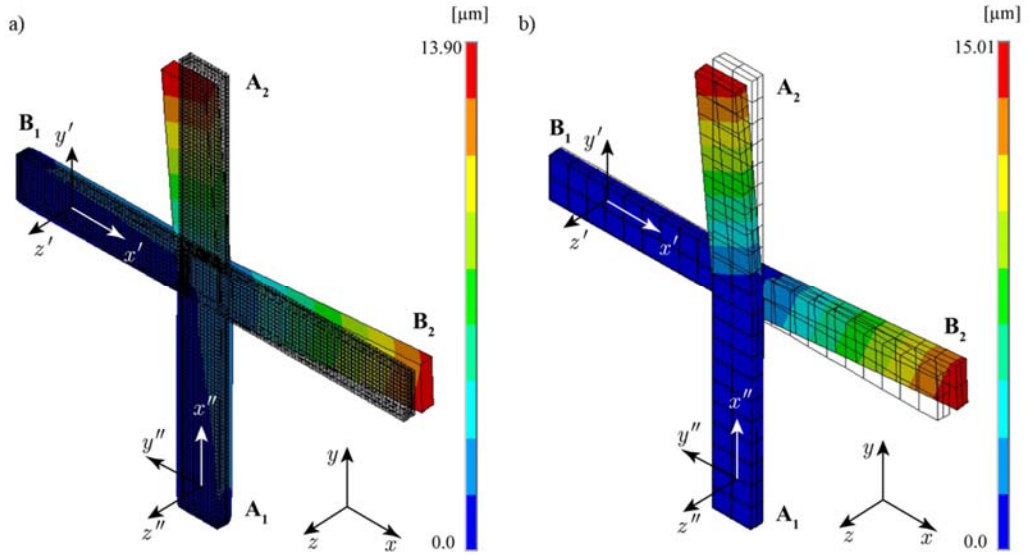


*Figure 3. The total deformation of fibers crossing at 90 degrees subjected to uniform moisture change of 15% with both the longitudinal and transverse hygroexpansion enabled: a) solid-shell model. b) beam model. The cross-sections at $\boldsymbol{A_1}$ and $\boldsymbol{B_1}$ are restrained in all dimensions, whereas $\boldsymbol{A_2}$ and $\boldsymbol{B_2}$ are unrestrained. The deformation contains an out-of-plane component despite the moisture change being uniform across the entire model. In the solid-shell model, the undeformed mesh is shown as an overlaid wireframe. For the case of a beam, the cross-section is visualized using a wireframe, although the element itself is a line.*

We investigate the contribution of the transverse hygroexpansion by fully disabling the longitudinal hygroexpansion of the fibers. Figure 4 shows the comparison. Both models predict approximately the same deformation. By comparing the results to those in Figure 3, it is clear that most of the observed out-of-plane deformation is caused by transverse hygroexpansion. It also shows that the multiscale approach captures the induced deformation state correctly since the results closely match those from the full 3D model using solid-shell elements.

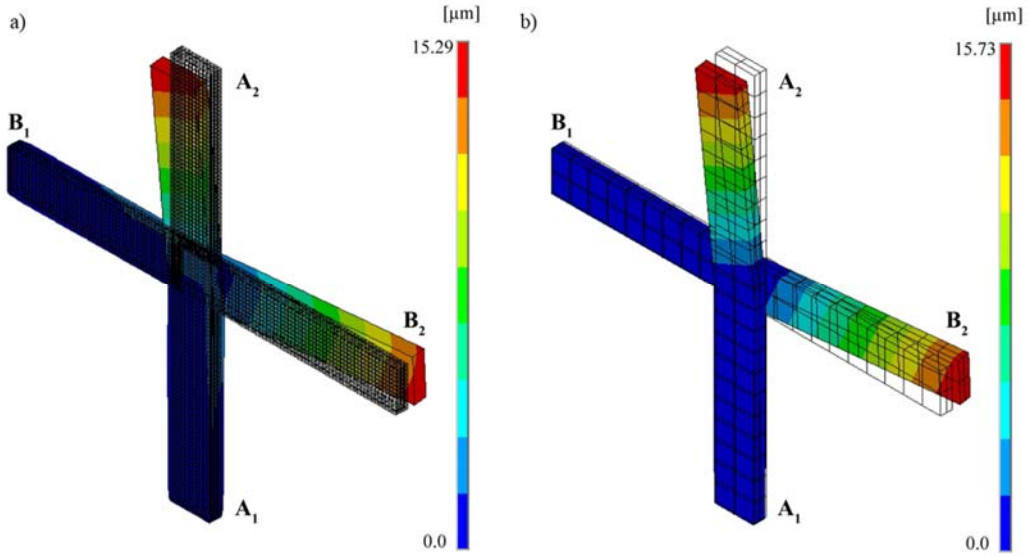


*Figure 4. The total deformation of fibers crossing at 90 degrees subjected to uniform moisture change of 15% with only transverse deformation enabled: a) solid-shell model. b) beam model. The cross-sections at $\boldsymbol{A_1}$ and $\boldsymbol{B_1}$ are restrained in all dimensions, whereas $\boldsymbol{A_2}$ and $\boldsymbol{B_2}$ are unrestrained. In the solid-shell model, the undeformed mesh is shown as an overlaid wireframe. For the case of a beam, the cross-section is visualized using a wireframe, although the element itself is a line.*

The reason the transverse deformation of the bond causes bending even with uniformly applied moisture can be seen in Figure 5 where the localized deformation at the fiber-to-fiber interface with a high strain gradient through the thickness of the fiber causes a bending moment which, in turn, causes out of plane deformation of the free fiber ends. Such deformation is only possible to capture by considering the full, 3D representation of the bond.

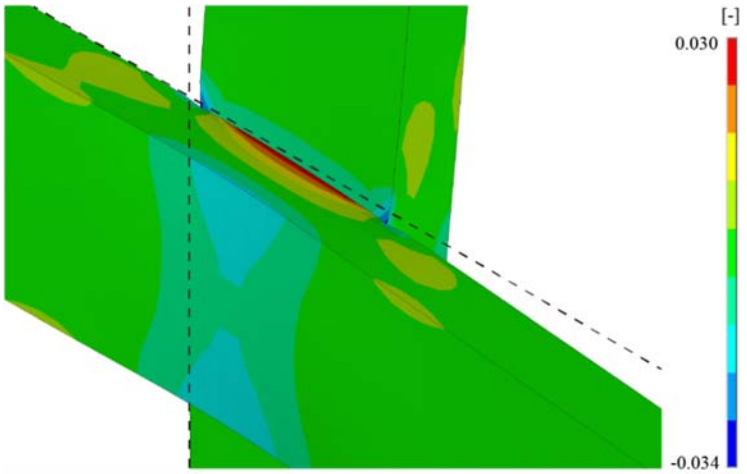


*Figure 5. The total equivalent strain in the bond region of the solid-shell model. The pronounced strain gradient between the bonded region and the fiber surface causes a bending moment which leads to out-of-plane deformation of the fiber crossing as shown in Figure 3.*

In a second test, we consider fibers crossing at an angle of 40 degrees. In addition, we prescribed the moisture gradient from top to the bottom varying linearly from 0 (bottom, $z_{\min}$ in the base shown in Figure 3) to 15% (top, $z_{\max}$ in the base shown in Figure 3). In this case, both fibers bend toward one side and both models yield similar results (Figure 6).

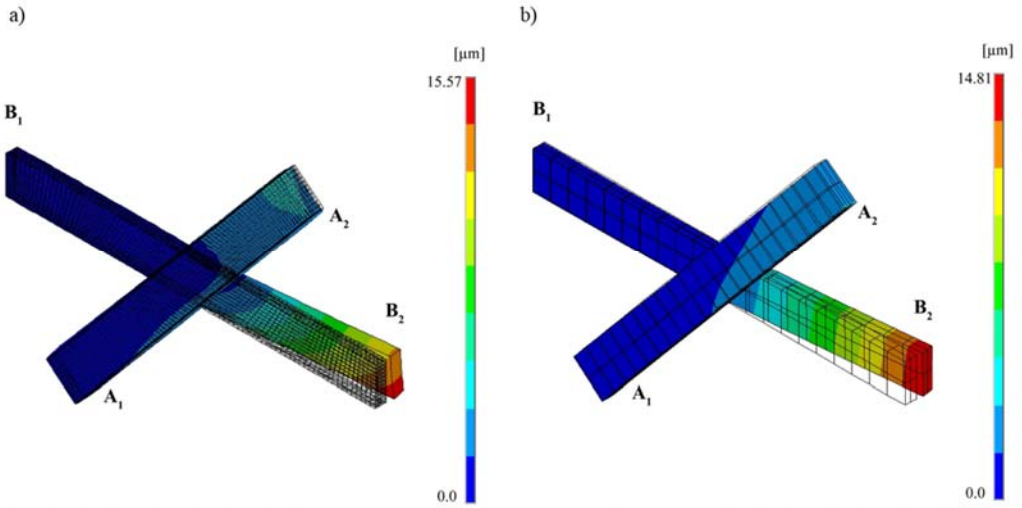


*Figure 6. The total deformation of fibers crossing at 40 degrees subjected to a moisture gradient varying linearly from 0 (bottom) to 15% (top) with both the longitudinal and transverse deformation enabled: a) solid-shell model. b) beam model. The cross-sections at $\boldsymbol{A_1}$ and $\boldsymbol{B_1}$ are restrained in all dimensions, whereas $\boldsymbol{A_2}$ and $\boldsymbol{B_2}$ are unrestrained. In the solid-shell model, the undeformed mesh is shown as an overlaid wireframe. For the case of a beam, the cross-section is visualized using a wireframe, although the element itself is a line.*

This simple model illustrates the importance of accounting for the 3D character of the fiber-to-fiber bond, even in the absence of moisture gradients. The most important result is the mechanism that causes out-of-plane deformations to appear: the large local strain gradient through the thickness of the bonded region.

**In-plane deformation**

Hygroexpansion is normally assessed using in-plane deformations in response to a uniform moisture change. We probe the difference between the reaction forces generated in-plane due to uniform moisture change for the 2D and the 3D bond model. The purpose is to examine the assumption that the bond deformation takes place under plane strain conditions. We consider the same fiber cross geometry (Figure 3) and properties (Table 1) but restrain all the degrees of freedom at the fiber ends. Table 2 shows the computed reaction force in the longitudinal direction of the fiber sampled at its end after the moisture change of 15 %.

*Table 2. The reaction force due to different combinations of deformation model at the bonds.*

| Reaction force [mN] | Longitudinal and transverse | Longitudinal only | Transverse only |
|---|---|---|---|
| 3D solid-shell | 13.6 | 12.2 | 1.4 |
| 2D bond model | 15.6 | 12.0 | **3.6** |
| 3D bond model | 13.5 | 12.1 | 1.4 |

This result shows that the 2D bond model overestimates the impact of the transverse deformation of the bond on the in-plane deformation of the fiber (marked in bold in Table 1). While the qualitative result is intuitive – the 2D bond model is inherently stiffer than the one which considers the elasticity of the fiber cross-section – the magnitude of the error suggests that treating the bond deformation as a plane-strain problem is not a reasonable assumption.

**Network-level simulation**

We compare the hygroexpansion coefficients for different degrees of structural anisotropy. To do this, a rectangular network of fibers 5x5 mm in size is created. We use the deposition procedure described below in order to create the network. The deposition algorithm can be outlined as follows:

1. The fiber geometry is sampled from fiber characterization data acquired with FiberLab (Valmet Fiber Image Analyzer), which is an apparatus for measuring fiber characteristics. It contains length, width, height, wall thickness, and curvature. The curvature is represented by an arc of constant curvature located in a single plane parallel to the deposition plane. The cross-sectional data is corrected using microtomography scans of a paper produced using the considered softwood Kraft pulp. The details of the correction are described elsewhere [19]. A summary of the fiber dimensions used in the study is presented in Table 3.
2. The fiber orientation is varied according to the normal distribution to achieve a desired degree of anisotropy, from isotropic in-plane orientation to orthotropic with a predominant orientation. The orientation is assessed by the ratio between elastic moduli measured in MD and CD.
3. The fiber spatial position before deposition onto the domain is chosen randomly.
4. The first fibers are deposited on the flat plane from above or below. For subsequent fibers, we first find the intersection between them and the previously deposited fibers in the plane (Figure 7a).
5. The found intersection points are raised to eliminate the penetration (Figure 7b). The contact search diameter depicted in the figure corresponds to the height of the fiber, which is smaller or equal to the width of the fiber.
6. The fiber geometry is smoothed to remove sharp transitions caused by the previous step (Figure 7c). During the smoothing, we control the maximum angle which the fibers can form with the MD-CD plane. In this study, we set the angle to 0 degrees, which means the fibers cannot bend at the contact point. While an angle of 0 degrees is unrealistic, it simplifies the interpretation of the results by removing one complexity of the network.
7. When the grammage (the basis weight or the weight per unit area) of the network reaches a prescribed value, the deposition procedure is stopped. The grammage used in this work is 100 $g/m^2$, which is relatively low but corresponds to the set of handsheets used to calibrate the measurements in [19].
8. The thickness of the network is evaluated using the procedure described in [19]. The thickness is brought to the target value by uniform scaling of the coordinates in the thickness direction with respect to the center plane of the network. The target value in this study was 80 micrometers. The scaling may result in interpenetrations, the effect of which are zeroed out during the subsequent computations.

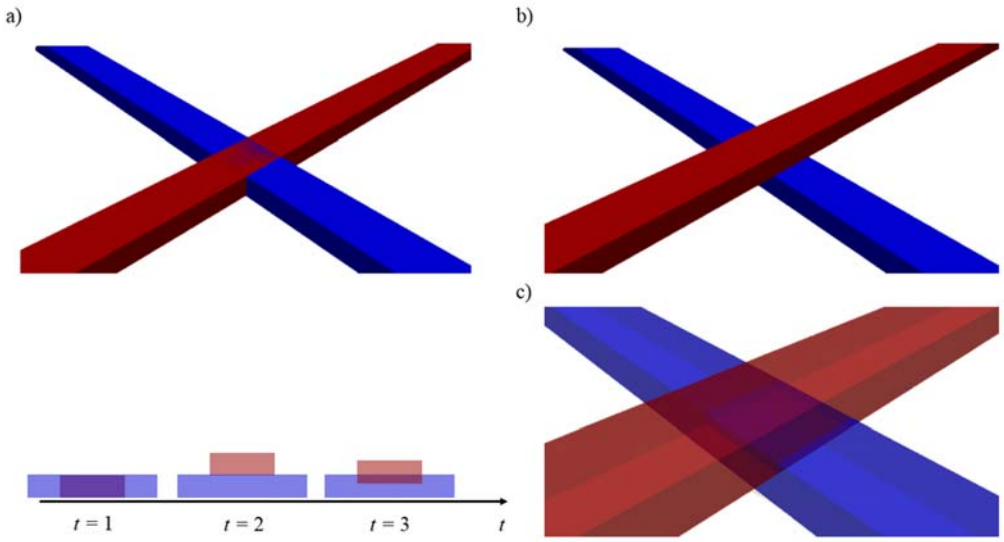


*Figure 7. Steps in deposition procedure: (a) An intersection is found between two fibers. (b) The second fiber to be deposited is raised to remove the interpenetration. (c) The complete structure is uniformly compressed to achieve the target thickness of the network. This results in some interpenetration, which is resolved during the solution phase.*

After generation of the geometry, the fibers are represented with a fine mesh of curved segments and imported into a custom finite element code. The segments are converted into cubic splines and meshed with beam elements with sufficient mesh density assessed with mesh convergence studies by observing the impact of the mesh size on the computed elastic modulus of the network.

*Table 3. Summary of the fiber data used in network simulations.*

| | **Mean** | **SD** |
|---|---|---|
| Fiber length, mm | 2.34 | 0.90 |
| Fiber width, $\mu$m | 23.83 | 7.09 |
| Fiber wall thickness, $\mu$m | 3.96 | 1.90 |
| Fiber cross-section width-to-height ratio, [-] | 2.9 | 1.72 |
| Fiber shape factor, [-] | 0.945 | 0.015 |
| Maximum interface angle[1], ° | 0 | - |
| Radius swelling factor[2], [-] | 0.78 | 0.68 |
| Wall thickness swelling factor[3], [-] | 0.528 | 0.31 |

[1] *Defined in [19].*
[2] *The ratio between the dry and wet measured radius.*
[3] *The ratio between the dry and wet measured wall-thickness.*

The fiber constitutive law is anisotropic plasticity with a bilinear isotropic hardening law. Debonding of fiber-to-fiber bonds is not considered. The material parameters, as well as hygroexpansion coefficients, are listed in Table 4.

*Table 4. Fiber material parameters used in the network simulation.*

| Elastic modulus, GPa | Tangent modulus, GPa | Yield stress, MPa | Longitudinal hygroexpansion Coefficient, - | Transverse hygroexpansion Coefficient, - |
|---|---|---|---|---|
| 30 | 6 | 100 | 0.03 | 0.6 |

A series of simulations are carried out for networks with varying degree of anisotropy. First, the square network is constrained in all the degrees of freedom at two opposite ends leaving the other two unconstrained. A prescribed displacement is applied at one of the constrained ends to extract the elastic modulus. The network is then rotated 90 degrees and the procedure is repeated to extract the elastic modulus in the cross-direction.

The same networks are subjected to a further test in which the network can shrink in both directions. The edges are constrained in the out-of-plane direction only and the minimum set of the translational constraints are applied to restrict the rigid body motion. The recorded displacements are converted into strains and the hygroexpansion coefficients are calculated accordingly. We perform the test with a 2D and then a 3D representation of the fiber bonds. Figure 8 shows the comparison between the tests through the dependence of hygroexpansion coefficient on the degree of anisotropy, which is in this case expressed through the ratio between the elastic moduli in the orthogonal directions referred to as MD and CD for simplicity of interpretation.

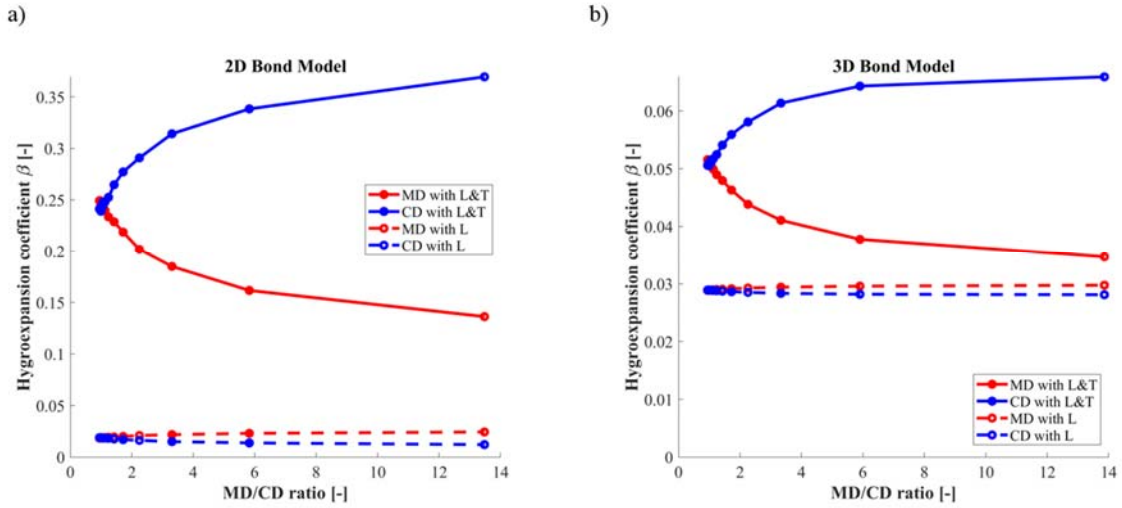


*Figure 8. The dependency of the hygroexpansion coefficients on the anisotropy for different modes of fiber-bond formulations: a) 2D bond model; b) 3D bond model. Note the difference in y-axis scale.*

There are several important findings from these results. First, the 2D bond model drastically overestimates the hygroexpansion. Prohibiting strain gradients across the bond's thickness, as is the case for the 2D model, leads the transverse fiber hygroexpansion to contribute too much to the network hygroexpansion. That the transverse hygroexpansion specifically is the one which is overestimated may be seen by observing the similar level of hygroexpansion due to longitudinal fiber expansion (L) but a significantly higher hygroexpansion when the transverse fiber hygroexpansion is also considered (L+T). Another interesting finding is that in the 3D bond model the contribution of the longitudinal deformation of the fibers is as large as the transverse even for highly oriented sheets and this contribution remains constant regardless the degree of anisotropy. This could be detected by disabling the transverse fiber deformation, an experiment which cannot be conducted in reality. This observation corroborates one of Uesaka's conclusions [9] about the importance of longitudinal hygroexpansion of the fibers.

The final application considered is curl. We restrain one side of the sheet, apply periodic boundary conditions to the opposite side and keep one of the sides free. We prescribe a linearly varying moisture content which reaches 15%

on one side and remains zero on the other. The moisture is varied through the integration points of the beam. The size of the considered strip is 10x2 mm. The strip is taken from a network with an isotropic in-plane orientation of the fibers. First, we made sure that there is no width dependency and compare the result with a wider strip 10x4 mm in size. Figure 9 shows that the strip develops a pronounced curl and increasing width does not affect the magnitude of out-of-plane deformation. Due to periodic boundary conditions, the network is not allowed to develop the curl in the opposite direction.

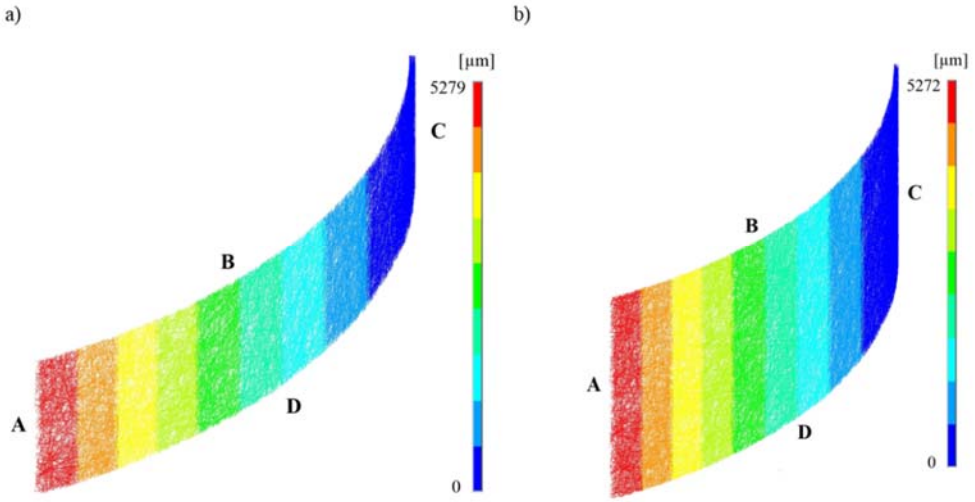


*Figure 9. Out-of-plane deformation of the sheet in response to a linear moisture gradient with the 3D bond model. Each fiber is shown as a line. The effect of the size: a) 10x2 mm, the reference sample; b) 10x4 mm, the wider sample. In these simulations, edges denoted **A** are unrestrained, **B** and **D** are coupled through a periodic boundary conditions, and edges **C** are constrained in all degrees of freedom.*

We consider the individual contribution of longitudinal and transverse deformation of the fibers to the out-of-plane deformation. By comparing the result in Figure 10 with Figure 9, we see that transverse deformation of the dominates in creating the curl. Furthermore, the driving force behind curl appears to be found in the bonds.

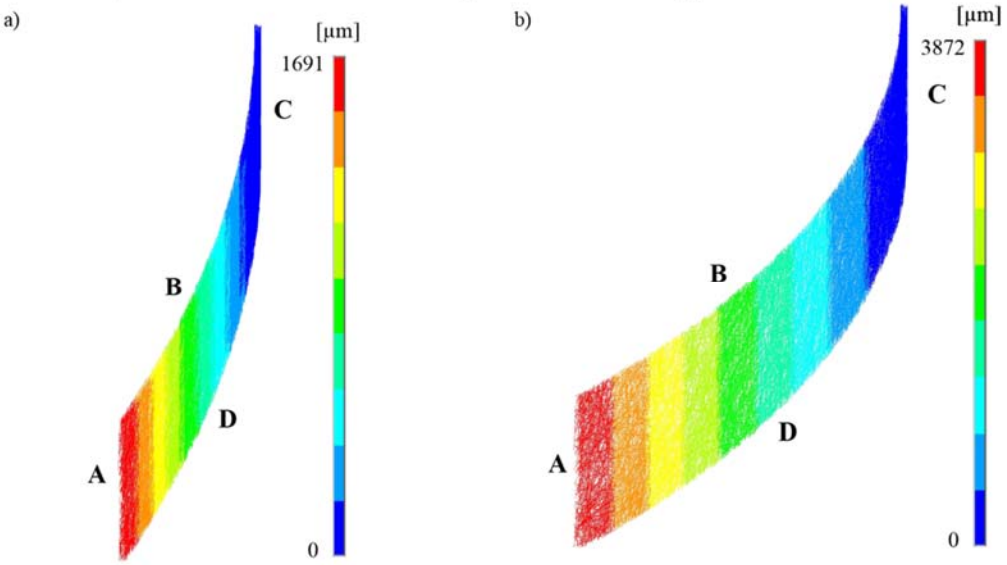


*Figure 10. Out-of-plane deformation of the sheet in response to a linear moisture gradient with the 3D bond model. The effect of the fiber-level deformation: a) only longitudinal hygroexpansion; b) only transverse hygroexpansion. In these simulations, edges denoted **A** are unrestrained, **B** and **D** are coupled through a periodic boundary conditions, and edges **C** are constrained in all degrees of freedom.*

This result can be compared with simulations where the bond is considered a purely 2D structure. We do so in Figure 11. The view is the same as in Figure 10, yet the deformation mode is completely changed, and the extent of out-of-plane deformation with only transverse hygroexpansion on the bond level (Figure 11b) is an order of magnitude smaller. Furthermore, it no longer has a distinct curl character. The reason the out-of-plane deformation obtained in response to only longitudinal deformation of the bond changed too, in comparison to Figure 10b, can be explained by the fact that in the 2D sub-model of the bond, the moisture gradient is not considered. It was only considered in the rest of the beams in the 3D structure of the network while the moisture in the fibers of the 2D sub-model was taken in the middle and is considered to be constant through the thickness of the corresponding fibers.

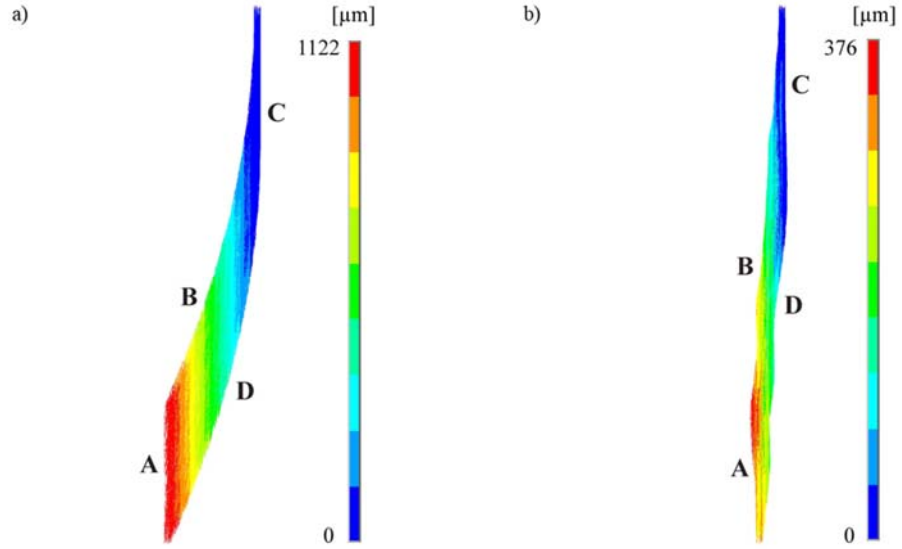


*Figure 11. Out-of-plane deformation of the sheet in response to a linear moisture gradient with the 2D bond model. The effect of the fiber-level deformation: a) only longitudinal hygroexpansion; b) only transverse hygroexpansion. In these simulations, edges denoted **A** are unrestrained, **B** and **D** are coupled through a periodic boundary conditions, and edges **C** are constrained in all degrees of freedom.*

## CONCLUSIONS

We present a comprehensive framework for network level micromechanical modeling of the hygroscopic deformations in paper. The framework consists of a concurrent multiscale model where fibers are idealized as beams while the bonds are resolved using a fully three-dimensional sub-model. The framework is verified against an entirely volumetric description of the fibers and bonds and is able to make accurate predictions at a considerably lower computational cost, enabling us to study large networks.

The geometrical configuration of the bonds is essential in developing the out-of-plane deformations. Comparing the results from 3D fiber-to-fiber bond modeling to those obtained using a 2D model for the bonds while still having a 3D structure for the network, we find that only the 3D model can correctly capture and identify key characteristics of paper hygroexpansion, such as the out-of-plane deformation resulting from a strong through-thickness strain gradient in the bonded region of the fiber. This out-of-plane deformation on the level of bonds can contribute materially to the development of curl, both elastic and permanent. In any case, it represents a new and highly relevant mechanism for the development of curl which up to now has been hidden by the comparatively coarse (but essentially correct) explanation of two-sidedness and through-thickness moisture gradient. By decomposing the hygroexpansion of fibers and studying the transverse and longitudinal part in isolation, we demonstrate the importance of longitudinal hygroexpansion of the fiber for the development of in-plane hygroexpansion of the sheet. The part of the hygroexpansion in response to the longitudinal deformation of the fibers is essentially unaffected by the in-plane anisotropy of the sheet.

**ACKNOWLEDGMENTS**

The financial support by the Austrian Federal Ministry of Science, Research and Economy and the National Foundation for Research, Technology, and Development is gratefully acknowledged. The computational resources were provided by the Swedish National Infrastructure for Computing (SNIC) at HPC2N, Umeå (Project SNIC2017-1-175).

**REFERENCES**

1. Niskanen, K., *Mechanics of paper products*. 2012: Walter de Gruyter.
2. Carlsson, L., *Out-of-plane hygroinstability of multi-ply paperboard.* Fibre Science and Technology, 1981. **14**(3): p. 201-212.
3. Mark, R.E., et al., *Handbook of Physical Testing of Paper: Volume 1*. 2001: Crc Press.
4. Lu, W. and L.A. Carlsson, *Influence of viscoelastic behavior on curl of paper.* Mechanics of Time-Dependent Materials, 2001. **5**(1): p. 79-100.
5. Page, D. and P. Tydeman, *A new theory of the shrinkage, structure and properties of paper.* Formation and Structure of Paper, 1962. **1**: p. 397-425.
6. Nanko, H. and J. Wu. *Mechanisms of paper shrinkage during drying*. in *International Paper Physics Conference, Niagara-on-the-Lake, Canada*. 1995.
7. Nanko, H. and Y. Tada. *Mechanism of hygroexpansion of paper*. in *International Paper Physics Conference*. 1995.
8. Uesaka, T. and D. Qi, *Hygroexpansivity of paper-Effects of fibre-to-fibre bonding.* Journal of pulp and paper science, 1994. **20**(6).
9. Uesaka, T., *General formula for hygroexpansion of paper.* Journal of Materials Science, 1994. **29**(9): p. 2373-2377.
10. Dvorak, G.J. and Y. Benveniste, *On transformation strains and uniform fields in multiphase elastic media.* Proc. R. Soc. Lond. A, 1992. **437**(1900): p. 291-310.
11. Salminen, L., et al., *Simulation of network shrinkage.* Nordic Pulp & Paper Research Journal, 2002. **17**(2): p. 105-110.
12. Bosco, E., R. Peerlings, and M. Geers, *Hygro-mechanical properties of paper fibrous networks through asymptotic homogenization and comparison with idealized models.* Mechanics of Materials, 2017. **108**: p. 11-20.
13. Bosco, E., et al., *On the role of moisture in triggering out-of-plane displacement in paper: from the network level to the macroscopic scale.* International Journal of Solids and Structures, 2018. **154**: p. 66-77.
14. Motamedian, H.R. and A. Kulachenko, *Simulating the hygroexpansion of paper using a 3D beam network model and concurrent multiscale approach.* International Journal of Solids and Structures, 2018.
15. Sellén, C. and P. Isaksson, *A mechanical model for dimensional instability in moisture-sensitive fiber networks.* Journal of Composite Materials, 2014. **48**(3): p. 277-289.
16. Ibrahimbegović, A., *On finite element implementation of geometrically nonlinear Reissner's beam theory: three-dimensional curved beam elements.* Computer methods in applied mechanics and engineering, 1995. **122**(1-2): p. 11-26.
17. Motamedian, H.R. and A. Kulachenko, *Rotational Constraint between Beams in 3-D Space.* Mechanical Sciences, 2018. **9**(2): p. 373-387.
18. Kulachenko, A. and T. Uesaka, *Direct simulations of fiber network deformation and failure.* Mechanics of Materials, 2012. **51**: p. 1-14.
19. Borodulina, S., H.R. Motamedian, and A. Kulachenko, *Effect of fiber and bond strength variations on the tensile stiffness and strength of fiber networks.* International Journal of Solids and Structures, 2018. **154**: p. 19-32.
20. Hauptmann, R. and K. Schweizerhof, *A systematic development of 'solid-shell' element formulations for linear and non-linear analyses employing only displacement degrees of freedom.* International Journal for Numerical Methods in Engineering, 1998. **42**(1): p. 49-69.